



Article

Fractal Analysis on the Mapping Relationship of Conductivity Properties in Porous Material

Cheng Li ¹, Yao Xu ¹, Zhouting Jiang ¹, Boming Yu ^{2,*} and Peng Xu ^{1,*} ¹ College of Science, China Jiliang University, Hangzhou 310018, China² Vebleo Fellow, School of Physics, Huazhong University of Science and Technology, Wuhan 430074, China

* Correspondence: yubm_2012@hust.edu.cn (B.Y.); xupeng@cjlu.edu.cn (P.X.)

Abstract: The mapping relationships between the conductivity properties are not only of great importance for understanding the transport phenomenon in porous material, but also benefit the prediction of transport parameters. Therefore, a fractal pore-scale model with capillary bundle is applied to study the fluid flow and heat conduction as well as gas diffusion through saturated porous material, and calculate the conductivity properties including effective permeability, thermal conductivity and diffusion coefficient. The results clearly show that the correlations between the conductivity properties of saturated porous material are prominent and depend on the way the pore structure changes. By comparing with available experimental results and 2D numerical simulation on Sierpinski carpet models, the proposed mapping relationships among transport properties are validated. The present mapping method provides a new window for understanding the transport processes through porous material, and sheds light on oil and gas resources, energy storage, carbon dioxide sequestration and storage as well as fuel cell etc.

Keywords: porous material; fractal geometry; permeability; thermal conductivity; diffusivity; mapping relationship



Citation: Li, C.; Xu, Y.; Jiang, Z.; Yu, B.; Xu, P. Fractal Analysis on the Mapping Relationship of

Conductivity Properties in Porous Material. *Fractal Fract.* **2022**, *6*, 527.

<https://doi.org/10.3390/fractalfract6090527>

Academic Editors: Gianina Dobrescu, Carlo Cattani, Florica Papa and Razvan State

Received: 5 August 2022

Accepted: 13 September 2022

Published: 17 September 2022

Publisher's Note: MDPI stays neutral with regard to jurisdictional claims in published maps and institutional affiliations.



Copyright: © 2022 by the authors. Licensee MDPI, Basel, Switzerland. This article is an open access article distributed under the terms and conditions of the Creative Commons Attribution (CC BY) license (<https://creativecommons.org/licenses/by/4.0/>).

1. Introduction

The conductivity properties including permeability, thermal conductivity and diffusivity are commonly used to characterize the transport processes through porous material, they are of great significance for oil and gas energy, geothermal resources, nuclear waste disposal, fuel cells, MEMS design, fibers, building materials, energy storage and drying technologies, etc. [1,2]. Since these transport properties strongly depend on the microstructures of porous material, a few theoretical and experimental studies have shown that there is an evident relationship among the permeability, thermal conductivity and diffusivity [3–5].

Zerrouki et al. [6] studied the petrophysical parameters of dry core samples of the Hamra quartzite reservoir, and presented a weak correlation for the thermal conductivity and the permeability via the radial basis function neural network method. Zierfuss et al. [7] reported that the thermal conductivity of sedimentary rocks with large pores rises with the increase of the permeability. Anand et al. [8] conducted a regression analysis on the thermal conductivity and physical properties of dry sandstone, and proposed a quantitative correlation among the thermal conductivity and porosity, density and permeability of dry sandstone. Mielke et al. [9] measured the thermal conductivity and permeability of rock cores from the Willerkai geothermal field in New Zealand, and predicted that the thermal conductivity and permeability were negatively correlated. Popov et al. [10] used the measured thermal conductivity to predict the permeability of the rock and its spatial distribution along the well, and found that the relative change in thermal conductivity of the rock after water saturation was positively correlated with the logarithm of the permeability, where the correlation coefficient was between 0.7 and 0.9. While, Duchkov et al. [11] reported a negative correlation between the thermal conductivity and the logarithm of

permeability in sandstone with siltstone. Wang et al. [12] proposed a quadratic function for the thermal conductivity and permeability of water-permeable cement concrete based on measurement results.

Pant et al. [13] related the permeability tortuosity to the diffusion tortuosity, and developed a permeability method to estimate the diffusivity. Villani et al. [14] measured the oxygen permeability and diffusivity of concrete by the oxygen permeability index method and Lawrence method, respectively. They showed that the oxygen permeability was almost linearly related to the diffusivity under the same humidity condition for the same proportion of concrete. Salvoldi et al. [15] presented a linear positive correlation between the effective diffusivity of carbon dioxide and the oxygen permeability in concrete with different water-cement ratio. Wang et al. [16] and Li et al. [17] proposed a positive correlation between the effective diffusion coefficient and permeability of methane in oil sands. Hosoya et al. [18] observed that the permeability of porous membranes was positively correlated with diffusivity. Reinecke et al. [19] established an exponent correlation between the gas permeability of the variable saturated porous material and the Knudsen diffusivity. Chen et al. [20] stated that the diffusivity was positively correlated with the permeability, and they found that the increase rate of diffusivity was small under low permeability and it is large under high permeability.

Although a few empirical and semi-empirical correlations between conductivity properties were proposed, they are even contradictory with each other and only validated for specific types of porous materials. In addition, the physical meanings of the empirical parameters in these correlations are not clearly revealed. Since a lot of studies have shown that the irregular microstructures of porous material can be finely represented by fractal scaling laws [1,21–23], and thus the conductivity properties have been analyzed based on various fractal pore-scale models [24]. Therefore, a fractal pore-scale model with capillary bundle is employed to explore the mapping correlations between conductivity properties of saturated porous material.

2. Fractal Theory for Pore Structures

The probability density function (f) of pore/capillary size (λ) in porous material has been revealed to follow a fractal law [24]:

$$f(\lambda) = D_F \lambda_{\min}^{D_F} \lambda^{-(D_F+1)} \quad (1)$$

where D_F is the fractal dimension for pore area, λ_{\min} represents the minimum sizes. As the key parameter in fractal geometry, the value of pore area fractal dimension is within the range of 0 to 2 and 0 to 3 on a 2D area and a 3D volume, respectively. Yu et al. [24] proposed an analytical relationship between the fractal dimension and the porosity, that is $\phi = (\lambda_{\min}/\lambda_{\max})^{D_E - D_F}$, where D_E is the Euclidean dimension and λ_{\max} represents the maximum sizes. Therefore, the mean pore/capillary size is:

$$\lambda_{ave} = \int_{\lambda_{\min}}^{\lambda_{\max}} \lambda f(\lambda) d\lambda = \frac{D_F}{D_F - 1} \lambda_{\min} \left[1 - \phi^{(D_F-1)/(D_E-D_F)} \right] \quad (2)$$

A fractal model shown in Figure 1 was used to characterize the pore-scale geometrical structure of a homogenous porous medium. One-dimensional transport through parallel capillaries in a cubic representative element volume (REV) was assumed. Both the size and tortuosity of capillaries were assumed to follow fractal scaling laws. The capillary length indicates self-similar fractal law [24,25].

$$L_t(\lambda) = \lambda^{1-D_T} L_0^{D_T} \quad (3)$$

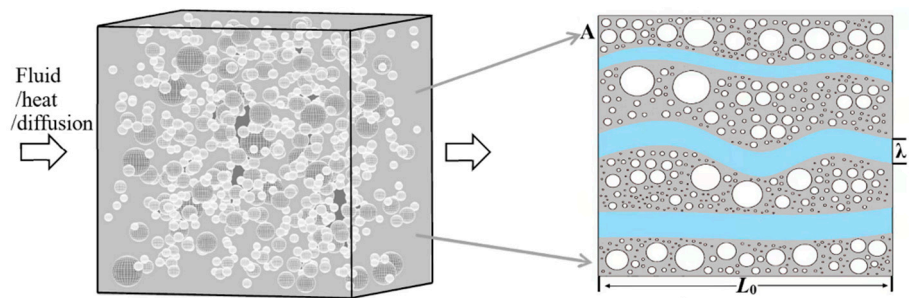


Figure 1. Fractal pore-scale model with tortuous capillary bundle of a REV.

The tortuous capillary length L_t is generally longer than the characteristic length L_0 . The convoluted extent of capillaries can be characterized by the tortuosity fractal dimension D_T , and the value of which falls between 1 and 2 in a 2D space. It can be calculated based on the mean tortuosity defined as $\tau_{ave} = L_t(\lambda_{ave})/L_0$:

$$D_T = 1 + \frac{\ln \tau_{ave}}{\ln(L_0/\lambda_{ave})} \quad (4)$$

The mean tortuosity can be estimated by the following analytical formula [24]:

$$\tau_{ave} = \frac{1}{2} \left[1 + \frac{1}{2} \sqrt{1-\phi} + \sqrt{1-\phi} \sqrt{\left(1/\sqrt{1-\phi} - 1\right)^2 + \frac{1}{4}} / (1 - \sqrt{1-\phi}) \right] \quad (5)$$

That is the mean tortuosity can be estimated with the porosity of porous material. On a 2D cross sectional area shown in Figure 1, the total pore area is:

$$A_p = \int_{\lambda_{\min}}^{\lambda_{\max}} \frac{\pi}{4} \lambda^2 f(\lambda) N_t d\lambda = \frac{\pi}{4} \frac{D_F}{2 - D_F} (1 - \phi) \lambda_{\max}^2 \quad (6)$$

where $N_t = (\lambda_{\max}/\lambda_{\min})^{D_F}$ is pore number on the cross sectional area. Then, the cross sectional area of the REV can be expressed as:

$$A = \frac{A_p}{\phi} = \frac{\pi}{4} \frac{D_F}{2 - D_F} \frac{1 - \phi}{\phi} \lambda_{\max}^2 \quad (7)$$

The representative length of the REV can be written as:

$$L_0 = \sqrt{A} = \left(\frac{\pi}{4} \frac{D_F}{2 - D_F} \frac{1 - \phi}{\phi} \right)^{1/2} \lambda_{\max} \quad (8)$$

3. Transport Properties of Porous Material

3.1. Effective Permeability

According to the modified Hagen-Poiseuille equation, the single phase flow rate (q) in a circular capillary channel depends on the capillary geometry (λ and L_t) and pressure drop along the capillary (ΔP) [24,26]:

$$q = \frac{\pi}{128} \frac{\Delta P}{\mu} \frac{\lambda^4}{L_t(\lambda)} \quad (9)$$

where μ is the incompressible Newtonian fluid viscosity. Based on the fractal scaling law of capillaries (Equations (1) and (3)), the flow rate across a 2D cross sectional area can be gotten from mass conservation:

$$Q = \int_{\lambda_{\min}}^{\lambda_{\max}} qf(\lambda) N_t d\lambda = \frac{\pi}{128} \left(\frac{4}{\pi}\right)^{D_T/2} \frac{(2-D_F)^{D_T/2}}{(3+D_T-D_F)D_F^{(D_T-2)/2}} \left(\frac{\phi}{1-\phi}\right)^{D_T/2} \frac{\Delta P}{\mu} \lambda_{\max}^3 \quad (10)$$

According to Darcy's law:

$$Q = A \frac{K \Delta P}{\mu L_0} \quad (11)$$

Then, by combining Equations (10) and (11), the effective permeability is gotten as:

$$K = \frac{1}{32} \left(\frac{4}{\pi}\right)^{(D_T-1)/2} \frac{(2-D_F)^{(D_T+1)/2}}{D_F^{(D_T-1)/2} (3+D_T-D_F)} \left(\frac{\phi}{1-\phi}\right)^{(D_T+1)/2} \lambda_{\max}^2 \quad (12)$$

The dimensionless permeability is defined and written as:

$$K^+ = \frac{K}{\lambda_{\max}^2} = \frac{1}{32} \left(\frac{4}{\pi}\right)^{(D_T-1)/2} \frac{(2-D_F)^{(D_T+1)/2}}{D_F^{(D_T-1)/2} (3+D_T-D_F)} \left(\frac{\phi}{1-\phi}\right)^{(D_T+1)/2} \quad (13)$$

The effective permeability of the porous material depends on the porosity and fractal dimensions for pore area and tortuosity, while it is independent of fluid properties and applied pressure gradient.

3.2. Thermal Conductivity

1D heat conduction and single phase fluid were assumed in this section. The thermal resistance can be calculated according to the Fourier heat transfer method [27].

$$r_f = \frac{4L_0^{D_T}}{\pi k_f \lambda^{1+D_T}} \quad (14)$$

where k_f is the fluid thermal conductivity. According to the parallel fractal capillary model shown in Figure 1, the thermal resistance for the fluid phase can be calculated as:

$$1/R_f = \int_{\lambda_{\min}}^{\lambda_{\max}} (1/r_f) f(\lambda) N_t d\lambda = k_f \left(\frac{4}{\pi}\right)^{D_T/2} \frac{(2-D_F)^{D_T/2}}{(1+D_T-D_F)D_F^{(D_T-2)/2}} \left(\frac{\phi}{1-\phi}\right)^{D_T/2} \left[1 - \phi^{(1+D_T-D_F)/(D_E-D_F)}\right] \lambda_{\max} \quad (15)$$

By the thermoelectric simulation method, the effective thermal conductivity can be expressed as:

$$k_e = \frac{L_0}{A} \left(\frac{1}{R_f} + \frac{1}{R_s}\right) \quad (16)$$

where the solid thermal resistance is generally estimated with:

$$R_s = \frac{L_0}{k_s(1-\phi)A} \quad (17)$$

Therefore, by combining Equations (7) and (15)–(17), the effective thermal conductivity is obtained:

$$k_e = k_f \left(\frac{4}{\pi}\right)^{(D_T-1)/2} \frac{(2-D_F)^{(D_T+1)/2}}{D_F^{(D_T+1)/2} (1+D_T-D_F)} \left(\frac{\phi}{1-\phi}\right)^{(D_T+1)/2} \left[1 - \phi^{(1+D_T-D_F)/(D_E-D_F)}\right] + k_s(1-\phi) \quad (18)$$

Then, the dimensionless thermal conductivity is:

$$k_e^+ = \frac{k_e}{k_f} = \left(\frac{4}{\pi}\right)^{(D_T-1)/2} \frac{(2-D_F)^{(D_T+1)/2}}{D_F^{(D_T+1)/2} (1+D_T-D_F)} \left(\frac{\phi}{1-\phi}\right)^{(D_T+1)/2} \left[1 - \phi^{(1+D_T-D_F)/(D_E-D_F)}\right] + \frac{k_s}{k_f} (1-\phi) \quad (19)$$

The effective thermal conductivity depends not only on pore structure (porosity, pore area fractal dimension and tortuosity fractal dimension) but also on the thermal conductivities of solid and fluid phases.

3.3. Diffusivity

The molecular diffusion under a concentration gradient (ΔC) through porous material was taken into account here. Thus, the gas diffusion flux through a capillary can be written as [28]:

$$j(\lambda) = \frac{\pi\lambda^2}{4} D_b \frac{\Delta C}{L_t(\lambda)} \quad (20)$$

where D_b is the bulk diffusion coefficient. Therefore, the diffusion flux through a cross section area in the REV is:

$$J = \int_{\lambda_{\min}}^{\lambda_{\max}} j(\lambda) f(\lambda) N_t d\lambda = D_b \Delta C \left(\frac{4}{\pi}\right)^{(D_T-2)/2} \frac{(2-D_F)^{D_T/2}}{(1+D_T-D_F)D_F^{(D_T-2)/2}} \left(\frac{\phi}{1-\phi}\right)^{D_T/2} \left[1 - \phi^{(1+D_T-D_F)/(D_E-D_F)}\right] \lambda_{\max} \quad (21)$$

Applying Fick's law on a porous sample results in:

$$J = D_e A \frac{\Delta C}{L_0} \quad (22)$$

Therefore, the effective gas diffusion coefficient can be deduced from Equations (7), (21) and (22) as:

$$D_e = D_b \left(\frac{4}{\pi}\right)^{(D_T-1)/2} \frac{(2-D_F)^{(D_T+1)/2}}{D_F^{(D_T-1)/2} (1+D_T-D_F)} \left(\frac{\phi}{1-\phi}\right)^{(D_T+1)/2} \left[1 - \phi^{(1+D_T-D_F)/(D_E-D_F)}\right] \quad (23)$$

The dimensionless diffusivity is:

$$D_e^+ = \frac{D_e}{D_b} = \left(\frac{4}{\pi}\right)^{(D_T-1)/2} \frac{(2-D_F)^{(D_T+1)/2}}{D_F^{(D_T-1)/2} (1+D_T-D_F)} \left(\frac{\phi}{1-\phi}\right)^{(D_T+1)/2} \left[1 - \phi^{(1+D_T-D_F)/(D_E-D_F)}\right] \quad (24)$$

The diffusivity is a function of porosity and fractal dimensions for pore area and tortuosity. It is similar to the permeability that the diffusivity only depends on the pore structures and it is independent of fluid properties and applied conditions.

4. The Numerical Simulation

The exactly self-similar Sierpinski carpet model was applied here, which can be generated by iterating over a square. As shown in Figure 2, the initial square of length L is equally divided into 9 squares, and then 2 parts are randomly removed. Same procedure is recursively applied on the remaining squares in the next stage. The porosity and pore fractal dimension are respectively $\phi_i = (7/9)^i$ and $D_F = \ln 7 / \ln 3 = 1.77124$, where i is the stage. For the incompressible Newtonian fluid flow through a 2D Sierpinski carpet, the inertial term in the Navier-Stokes equation can be neglected if the Reynolds number is low and the governing equations are:

$$\rho \nabla \cdot \mathbf{u} = 0 \quad (25)$$

$$\nabla \cdot \left[P \mathbf{I} + \mu (\nabla \mathbf{u} + (\nabla \mathbf{u})^T) \right] + \mathbf{F} = 0 \quad (26)$$

$$\rho C_p \mathbf{u} \cdot \nabla T = \nabla \cdot (k \nabla T) \quad (27)$$

$$\mathbf{u} \cdot \nabla C_j = R_j + \nabla \cdot (D_j \nabla C_j) \quad (28)$$

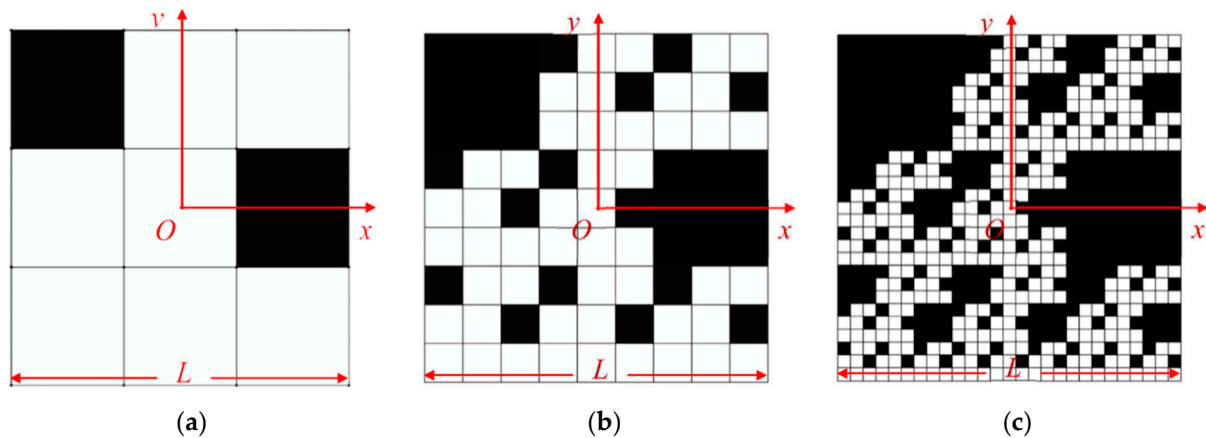


Figure 2. The generation procedure of 2D Sierpinski carpet model: (a) $i = 1$; (b) $i = 2$; (c) $i = 3$ (white and black areas represent pore and solid phases, respectively).

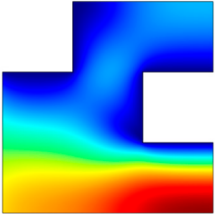
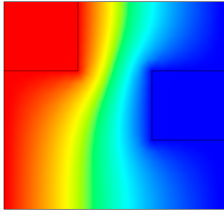
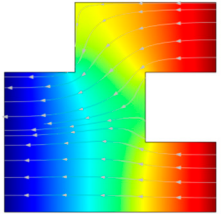
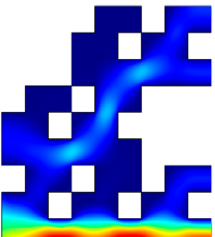
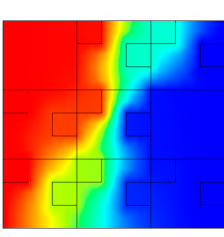
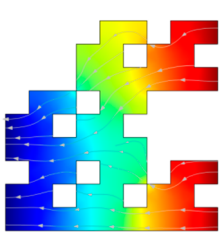
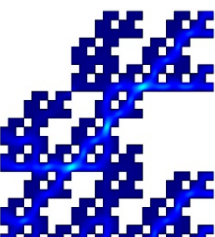
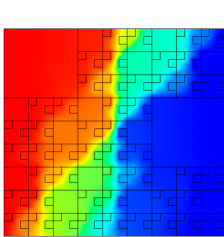
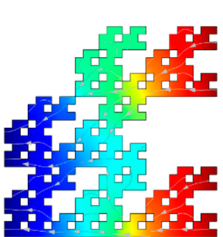
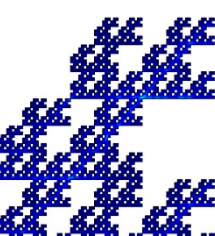
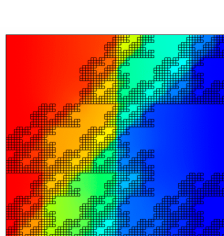
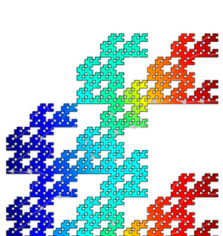
The symbols ρ , P , k , T , C_p , C_j , R_j , D_j , \mathbf{u} , \mathbf{F} , \mathbf{I} are fluid density, pressure, thermal conductivity, temperature, specific heat capacity, concentration, molar flux, diffusion coefficient, velocity vector, volume force vector, unit diagonal matrix, respectively.

Numerical simulations of the single-phase percolation, heat conduction and gas diffusion were carried out using COMSOL Multiphysics based on the finite element method. The creeping flow module, heat transfer in solids module and diluted species transport module were employed to solve the gas flow, heat conduction, and gas diffusion in steady state through the 2D Sierpinski carpet model, respectively. Oxygen with density $\rho_f = 1.429 \text{ kg/m}^3$, viscosity $\mu_f = 2.05506 \times 10^{-5} \text{ Pa}\cdot\text{s}$, intrinsic thermal conductivity $k_f = 0.024 \text{ W/(m}\cdot\text{K)}$, specific heat capacity $C_{p,f} = 918 \text{ J/(kg}\cdot\text{K)}$, and the gaseous-diffusion coefficient $D_j = 1 \times 10^{-9} \text{ m}^2/\text{s}$ was adopted as the flow medium. Sandstone with density $\rho_s = 2600 \text{ kg/m}^3$, intrinsic thermal conductivity $k_s = 2.95 \text{ W/(m}\cdot\text{K)}$, and specific heat capacity $C_{s,f} = 800 \text{ J/(kg}\cdot\text{K)}$ was used as solid substrate. The pressure difference, temperature difference and concentration difference between the inlet and outlet were set to be 0.5 Pa, 10 K and 5 mol/m³, respectively. The symmetric boundary condition was used for the upper and lower layers. The mesh was controlled by a physical mesh, and the independency of grid density was also examined.

5. Results and Discussion

Available researches showed that the transport parameters of porous material are strongly dependent on multiple microstructure parameters including not only porosity but also fractal dimension as well as the self-similar range of pore size (ratio of minimum to maximum pore size) etc. The numerical results summarized in Table 1 show that the porosity decreases continuously with increased iteration stage i and the proportion of solid phase increases, which enhances the thermal conductivity of porous material and improves temperature uniformity. However, the increased flow and diffusion tortuosity will increase the resistance of the porous material, thus, the flow velocity and diffusion velocity decrease with the decrease of porosity.

Table 1. The velocity, temperature and concentration fields of Sierpinski carpet models.

Order	Porosity (%)	τ_{ave}	u (m/s)	T (K)	C (mol/m ³)
$i = 1$	77.78	1.16529			
$i = 2$	60.49	1.31212			
$i = 3$	47.05	1.51631			
$i = 4$	36.60	1.79652			

The effective permeability, thermal conductivity and diffusivity were estimated by Darcy's law, Fourier's law and Fick's first law, respectively. Figure 3 shows the relationships among the effective permeability, thermal conductivity and gas diffusivity by fractal model (Equations (12), (19) and (24)) and numerical simulation (Equations (25)–(28)). The thermal conductivity and gas diffusivity respectively indicates negative and positive correlations with the effective permeability of porous material with variable porosity (36.60–77.78%), which are consistent with experimental results [6,8–12,14–18,20]. As illustrated in Figure 3, the predicted results by the current model are in acceptable agreement with that by the numerical simulation. The predicted relationships among the effective permeability, thermal conductivity and gas diffusivity were compared with those by experiments [6,7,14–17] and empirical formulas [8,11,12,14,18–20]. Figure 4 shows that the predictions by the present model show fair agreement with experimental results comparing with available empirical formulas.

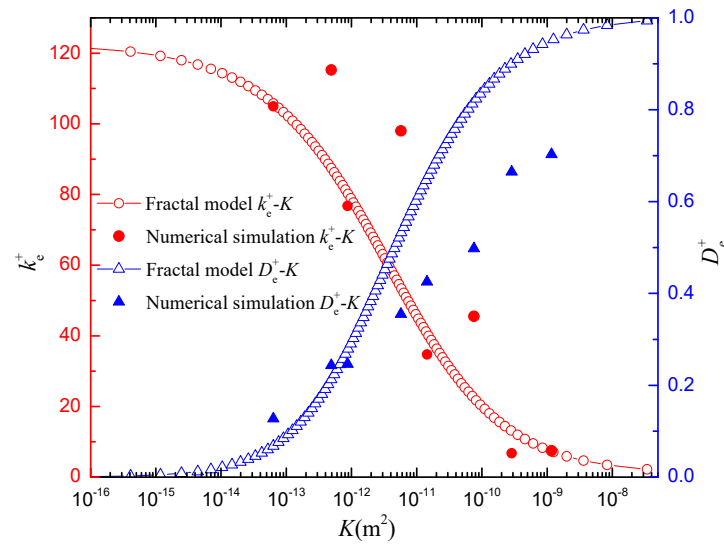


Figure 3. The mapping correlations among the effective permeability, thermal conductivity and gas diffusivity by fractal model and numerical simulation.

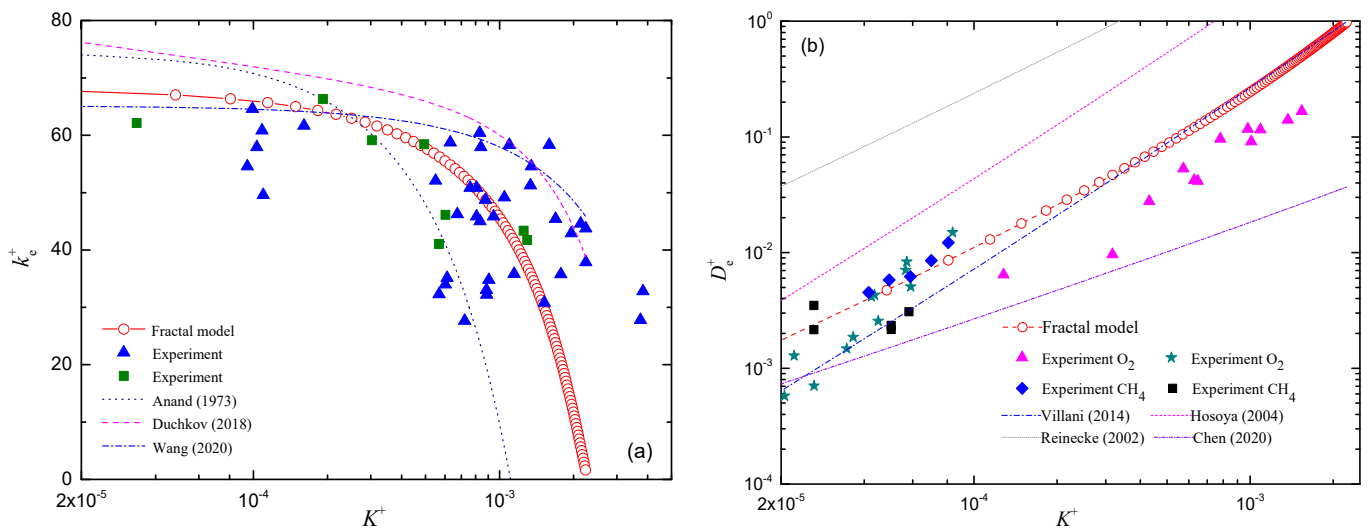


Figure 4. The comparison of mapping correlations among transport parameters between the present fractal model and available data: (a) $k_c^+ \sim K^+$ and (b) $D_c^+ \sim K^+$.

The influences of these parameters on the correlations of conductivity properties were also examined. Figure 5 indicates that the pore size range has important effect on the mapping correlations between transport parameters of porous material. As mentioned above, both the effective permeability and gas diffusivity increase with the increase of porosity, while the effective thermal conductivity decreases as the porosity increases. Thus, the thermal conductivity and gas diffusivity respectively show the negative and positive correlations with permeability of porous material with variable porosity. However, under certain porosity, the pore size range which causes the fractal dimension changing [27], may induce the changes of transport parameters. It can be clearly seen from Figure 6 that both effective thermal conductivity and gas diffusivity show positive correlation with the effective permeability of porous material with a certain porosity.

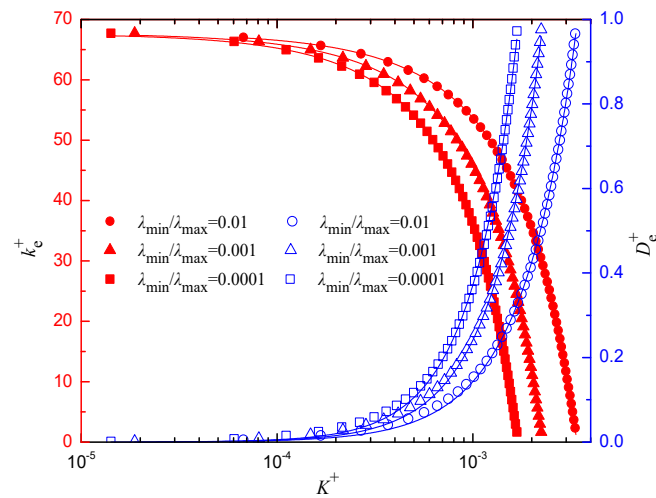


Figure 5. The influence of self-similar range of pore size on the mapping correlations of the effective permeability, thermal conductivity, and diffusivity of porous material with variable porosity.

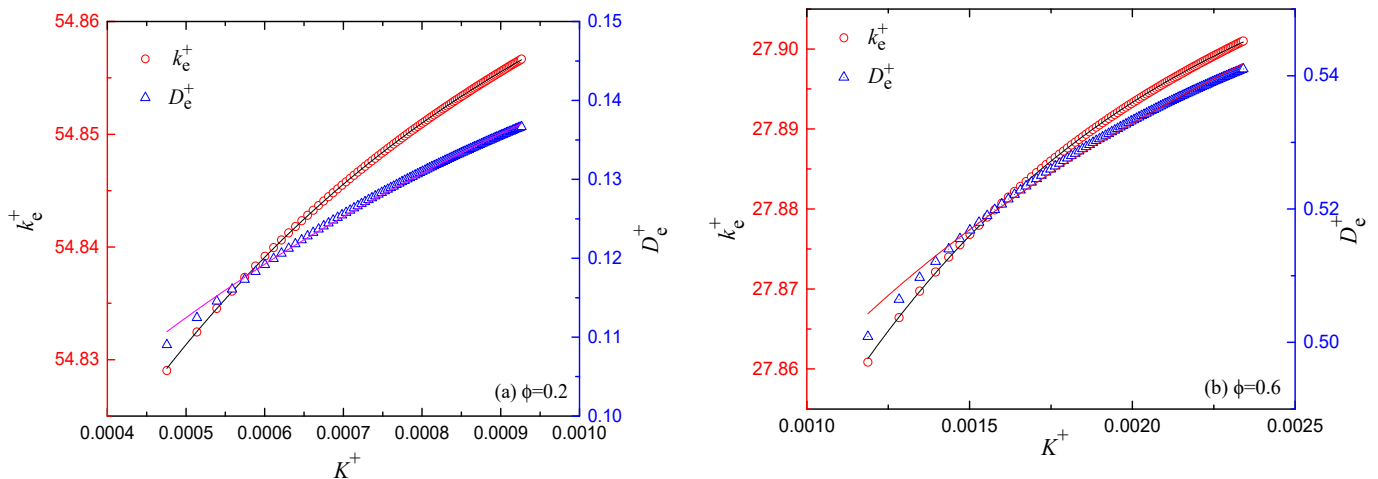


Figure 6. The mapping correlations of effective permeability, thermal conductivity, and diffusivity of porous material under certain porosity of (a) 0.2 and (b) 0.6.

Further calculations indicate that the effective thermal conductivity and effective permeability of porous material follow an exponential function:

$$k_e^+ = y_0 + A_1 e^{-K^+/t_1} \tag{29}$$

where y_0, A_1, t_1 are the fitting coefficients for the exponential function. Table 2 summarizes the fitting parameters in the exponential function for the cases shown in Figures 5 and 6, where the fitting correlation $R^2 > 0.99$. The ranges of porosity and pore size are 0~1 and $10^{-2} \sim 10^{-6}$, respectively.

The gas diffusivity and effective permeability of porous material were found to conform a power law function:

$$D_e^+ = a(K^+)^b \tag{30}$$

where a and b are the fitting coefficients of the power law function. Table 3 summarizes the fitting parameters in the power function between the gas diffusivity and effective permeability, and the fitting correlation $R^2 > 0.99$. The ranges of porosity and pore size are the same as that of Table 2.

Table 2. The parameters in the mapping correlation between thermal conductivity and effective permeability.

ϕ	$\lambda_{\min}/\lambda_{\max}$	y_0	A_1	t_1	R^2
0~1	10^{-2}	114.34104	-46.54972	-0.00378	0.99998
	10^{-3}	108.81465	-41.10519	-0.00233	0.99998
	10^{-4}	106.67414	-39.04452	-0.00169	0.99997
0.2	$10^{-6}\sim 10^{-2}$	54.87881	-0.11576	5.61052×10^{-4}	0.99996
0.4		49.39195	-0.18928	7.93047×10^{-4}	0.99990
0.6		27.92030	-0.18524	0.00104	0.99990

Table 3. The parameters in the mapping correlation between gas diffusivity and the effective permeability.

ϕ	$\lambda_{\min}/\lambda_{\max}$	a	b	R^2
0~1	10^{-2}	7.71754×10^3	1.57728	0.99947
	10^{-3}	3.32852×10^4	1.71317	0.99932
	10^{-4}	1.07199×10^5	1.82005	0.99921
0.2	$10^{-6}\sim 10^{-2}$	1.28611	0.32057	0.99973
0.4		1.10299	0.18885	0.99330
0.6		1.02776	0.10570	0.99440

6. Concluding Remarks

A pore-scale fractal model has been employed to study the transport process through porous material, and 2D numerical simulations have been also carried out on the Sierpinski carpet models by the finite element method. It has been found that the correlation between thermal conductivity and effective permeability follows an exponential function. They show a negative correlation with the change of the porosity of porous material, while they may indicate the positive correlation with invariable porosity and variable pore area fractal dimension. The gas diffusion coefficient positively correlated with the effective permeability of porous material, and they obey a power law function. The correlations between the transport properties of porous material are strongly dependent on the microstructures (i.e., porosity, fractal dimension and pore size range etc).

The proposed mapping relationship among the permeability, thermal conductivity and diffusivity can reveal the physical mechanisms of transport phenomenon in porous material, and this relationship can be also applied to predict the transport properties. For example, the thermal conductivity can be estimated from geophysical logs by the proposed correlation, since measuring thermal conductivity is generally difficult and time consuming. The present results may shed light on oil and gas resources, energy storage, carbon dioxide sequestration and storage, and fuel cell etc. However, it should be noted that the closed and non-communicative pores, variable cross-sectional area of capillary, contact thermal resistance etc. should be included in order to improve the prediction accuracy of the model.

Author Contributions: Conceptualization, P.X.; funding acquisition, P.X. and Z.J., methodology, B.Y.; supervision, P.X. and Z.J.; validation, C.L. and Y.X.; writing—original draft preparation, C.L. All authors have read and agreed to the published version of the manuscript.

Funding: This work was jointly funded by the Natural Science Foundation of China [grant numbers 51876196, 21873087], the Zhejiang Provincial Natural Science Foundation of China [grant numbers LR19E060001], the Fundamental Research Funds for the Provincial Universities of Zhejiang [grant number 2020YW13].

Data Availability Statement: All data are contained within the paper, and a report of any other data is not included.

Acknowledgments: The authors thank the referees for detailed reading and comments that were both helpful and insightful.

Conflicts of Interest: The authors declare no conflict of interest.

References

1. Xu, P.; Sasmito, A.; Mujumdar, A. *Heat and Mass Transfer in Drying of Porous Media*, 1st ed.; CRC Press: Boca Raton, FL USA, 2019; pp. 1–36.
2. Wu, Z.; Cui, C.; Yang, Y.; Zhang, C.; Wang, J.; Cai, X. A fractal permeability model of tight oil reservoirs considering the effects of multiple factors. *Fractal Fract.* **2022**, *6*, 153. [[CrossRef](#)]
3. Hu, B.; Wang, J.; Ma, Z.; Sang, S. Permeability and thermal conductivity models of shale matrix with a bundle of tortuous fractal tree-like branching micropore networks. *Int. J. Therm Sci.* **2021**, *164*, 106876. [[CrossRef](#)]
4. Xia, Y.; Wei, W.; Liu, Y.; Cai, Z.; Cai, J. A fractal-based approach to evaluate the effect of microstructure on the permeability of two-dimensional porous media. *Appl. Geochemistry.* **2021**, *131*, 105013. [[CrossRef](#)]
5. Li, C.; An, H.; Zhao, J.; Kang, Q.; Li, Z.; Carmeliet, J.; Shikazono, N.; Tao, W. Pore-scale modeling of complex transport phenomena in porous media-ScienceDirect. *Prog. Energy Combust. Sci.* **2022**, *88*, 100968.
6. Zerrouki, A.; Geraud, Y.; Diraison, M.; Ba, D. A Preliminary study of relationships between thermal conductivity and petrophysical parameters in Hamra Quartzites reservoir, Hassi Messaoud field (Algeria). *J. African Earth Sci.* **2019**, *151*, 461–471. [[CrossRef](#)]
7. Zierfuss, H.; Vliet, G. Laboratory measurements of heat conductivity of sedimentary rocks. *Am Assoc Pet Geol Bull.* **1956**, *40*, 2475–2488.
8. Anand, J.; Somerton, W.; Gomaa, E. Predicting thermal conductivities of formations from other known properties. *SPE* **1973**, *13*, 267–273. [[CrossRef](#)]
9. Mielke, P.; Bignall, G.; Sass, I. Permeability and Thermal Conductivity Measurements of Near Surface Units at the Wairakei Geothermal Field, New Zealand. In Proceedings of the World Geothermal Congress 2010, Bali, Indonesia, 25–29 April 2010.
10. Popov, Y.; Tertychnyi, V.; Romushkevich, R.; Korobkov, D.; Pohl, J. Interrelations between thermal conductivity and other physical properties of rocks: Experimental data. *Pure Appl. Geophys.* **2003**, *160*, 1137–1161. [[CrossRef](#)]
11. Duchkov, A.; Ayunov, D.; Rodyakin, S.; Chernysh, P. The study of the relationship between thermal conductivity and porosity, permeability, humidity of sedimentary rocks of the West Siberian Plate. *Georesources.* **2018**, *4*, 396–403.
12. Wang, H.; Zhang, A.; Shi, F.; Liu, J.; Cao, P.; Du, T.; Gu, H. Development of relationships between permeability coefficient and electrical and thermal conductivity of recycled aggregates permeable cement concrete. *Constr Build Mater.* **2020**, *254*, 119247. [[CrossRef](#)]
13. Pant, L.; Mitra, S.; Marc, S. Absolute permeability and Knudsen diffusivity measurements in PEMFC gas diffusion layers and micro porous layers. *J. Power Sources.* **2012**, *206*, 153–160. [[CrossRef](#)]
14. Villani, C.; Loser, R.; West, M.; Bella, C.; Lura, P.; Weiss, W. An inter lab comparison of gas transport testing procedures: Oxygen permeability and oxygen diffusivity. *Cem Concr Compos.* **2014**, *53*, 357–366. [[CrossRef](#)]
15. Salvoldi, B.; Beushausen, H.; Alexander, M. Oxygen permeability of concrete and its relation to carbonation. *Constr Build Mater.* **2015**, *85*, 30–37. [[CrossRef](#)]
16. Wang, X.; Zhao, X. An approach to measure tortuosity based on molecular diffusion theory. *Natural Gas Technology and Economy.* **2017**, *11*, 37–42, 82–83.
17. Li, Z.; Dong, M. Experimental study of carbon dioxide diffusion in oil-saturated porous media under reservoir conditions. *Ind. Eng. Chem. Res.* **2009**, *48*, 9307–9317. [[CrossRef](#)]
18. Hosoya, O.; Chono, S.; Saso, Y.; Juni, K.; Morimoto, K.; Seki, T. Determination of diffusion coefficients of peptides and prediction of permeability through a porous membrane. *J. Pharm. Pharmacol.* **2004**, *56*, 1501–1507. [[CrossRef](#)]
19. Reinecke, S.; Sleep, B. Knudsen diffusion, gas permeability, and water content in an unconsolidated porous medium. *Water Resour. Res.* **2002**, *38*, 1280–1296. [[CrossRef](#)]
20. Chen, L.; Hu, Z.; Xiong, W.; Duan, X.; Chang, J. Diffusion experiment of shale gas and mathematical model. *Nat. Gas Geosci.* **2020**, *31*, 1285–1293.
21. Katz, A.; Thompson, A. Fractal sandstone pores: Implications for conductivity and pore formation. *Phys Rev Lett.* **1985**, *54*, 1325–1328. [[CrossRef](#)]
22. Hasmy, A.; Olivi-Tran, N. Diffusivity and pore distribution in fractal and random media. *Phys. Rev. E.* **1999**, *59*, 3012–3015. [[CrossRef](#)]
23. Bonnet, E.; Bour, O.; Odling, N.; Davy, P.; Main, I.; Cowie, P.; Berkowitz, B. Scaling of fracture systems in geological media. *Rev Geophys.* **2001**, *39*, 347–383. [[CrossRef](#)]
24. Yu, B. Analysis of flow in fractal porous media. *Appl. Mech. Rev.* **2008**, *61*, 050801. [[CrossRef](#)]
25. Wheatcraft, S.; Tyler, S. An explanation of scale-dependent dispersivity in heterogeneous aquifers using concepts of fractal geometry. *Water Resour. Res.* **1988**, *24*, 566–578. [[CrossRef](#)]
26. Pfitzner, J. Poiseuille and his law. *Anaesthesia.* **1976**, *31*, 273–275. [[CrossRef](#)] [[PubMed](#)]
27. Fraisse, G.; Lazard, M.; Goupil, C.; Serrat, J. Study of a thermoelement's behaviour through a modelling based on electrical analogy. *Int. J. Heat Mass Transf.* **2010**, *53*, 3503–3512. [[CrossRef](#)]
28. Webb, S.; Pruess, K. The use of Fick's law for modeling trace gas diffusion in porous media. *Transp Porous Media.* **2003**, *51*, 327–341. [[CrossRef](#)]